



*Supplement of*

## **Evolution of crystallographic preferred orientations of ice sheared to high strains by equal-channel angular pressing**

**Qinyu Wang et al.**

*Correspondence to:* Chao Qi ([chao.qi@hpstar.ac.cn](mailto:chao.qi@hpstar.ac.cn))

The copyright of individual parts of the supplement might differ from the article licence.

**Table S1.** Sensitivity test of different thresholds for carbon signal.

	Threshold of carbon signal	undeformed	33_1p	19_2p	19_3p	21_4p	34_5p	38_6p
SPO (°)	1	N/A <sup>a</sup>	32	12	14	11	17	9
	2	N/A <sup>a</sup>	26	10	12	10	14	8
	4	N/A <sup>a</sup>	22	6	10	10	13	8
grain size (μm)	1	140	180	167	211	139	155	143
	2	154	195	186	222	137	168	149
	4	162	207	203	234	137	180	153

<sup>a</sup>No shape preferred orientation (SPO) analysis was performed on the undeformed samples.

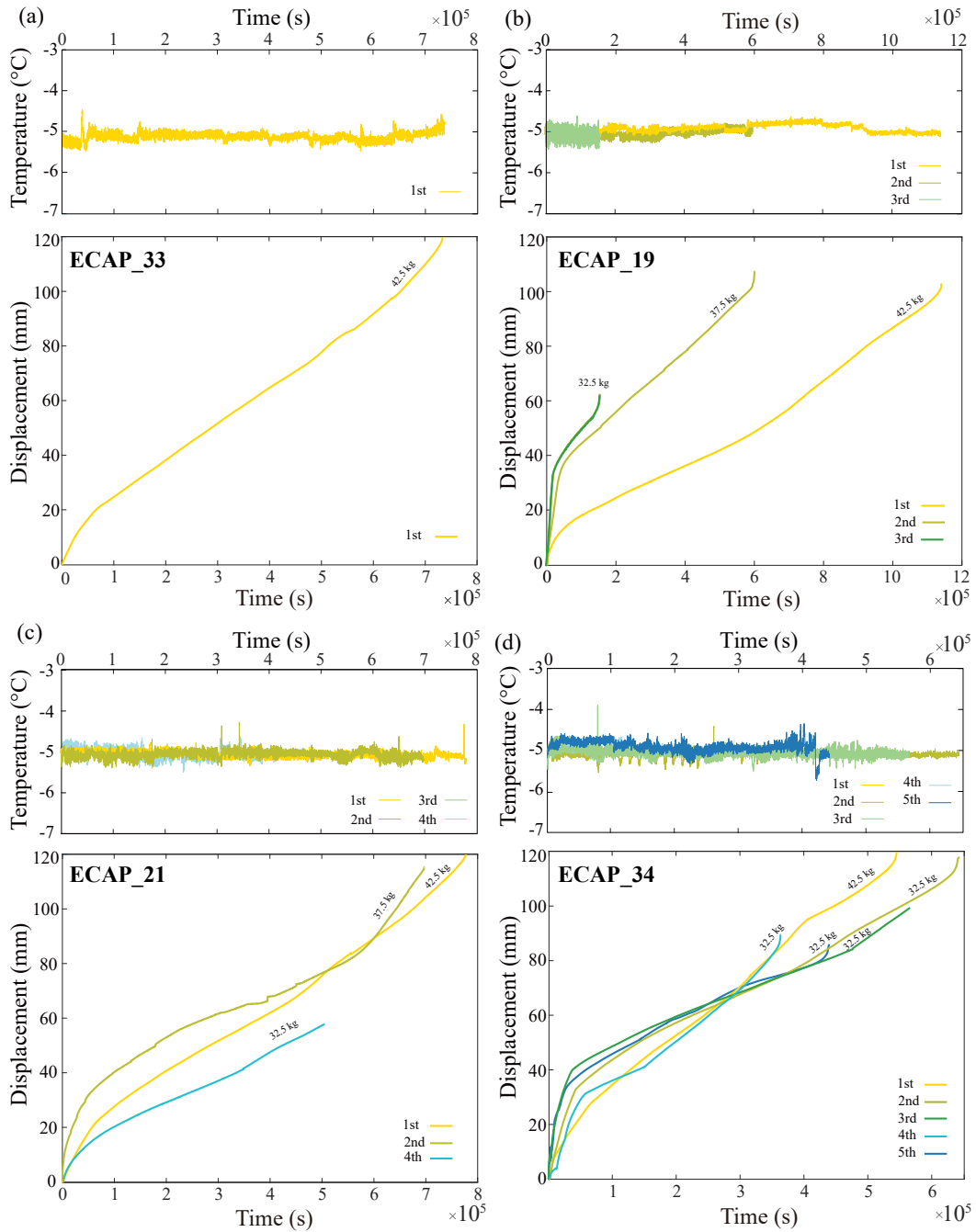


**Figure S1.** Plots of temperature and displacement versus time for all samples. The temperature is measured on the outer surface of the die, right at the corner. Warmer to cooler colors mark the 1st to the 5th pass, with cooler colors indicating a higher number of passes through the channels. The maximum load for each pass is noted next to the curve. (a) Sample ECAP\_33. (b) Sample ECAP\_19. (c) Sample ECAP\_21. The temperature and displacement data of the 3rd pass were not preserved. (d) Sample ECAP\_34.

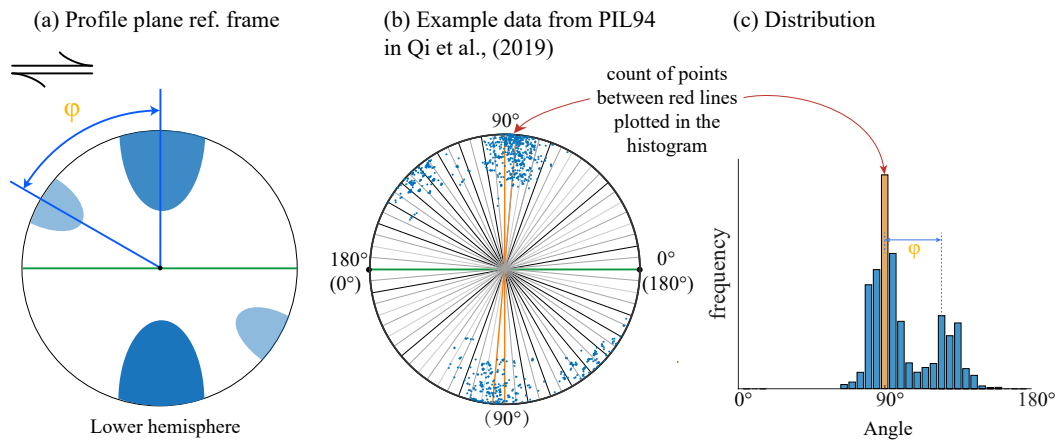


**Figure S2.** An illustration of the determination of angle  $\varphi$ . (a) Typical two-cluster distribution of  $c$  axes on stereonets within the profile plane reference frame (plane normal to the shear plane and parallel to the shear direction). (b) A schematic illustration explaining the method used to quantify the distribution of  $c$  axes. (c) A histogram of  $c$  axes plotted in a histogram, illustrating the angle  $\varphi$  between the two clusters of  $c$  axes.



undeformed

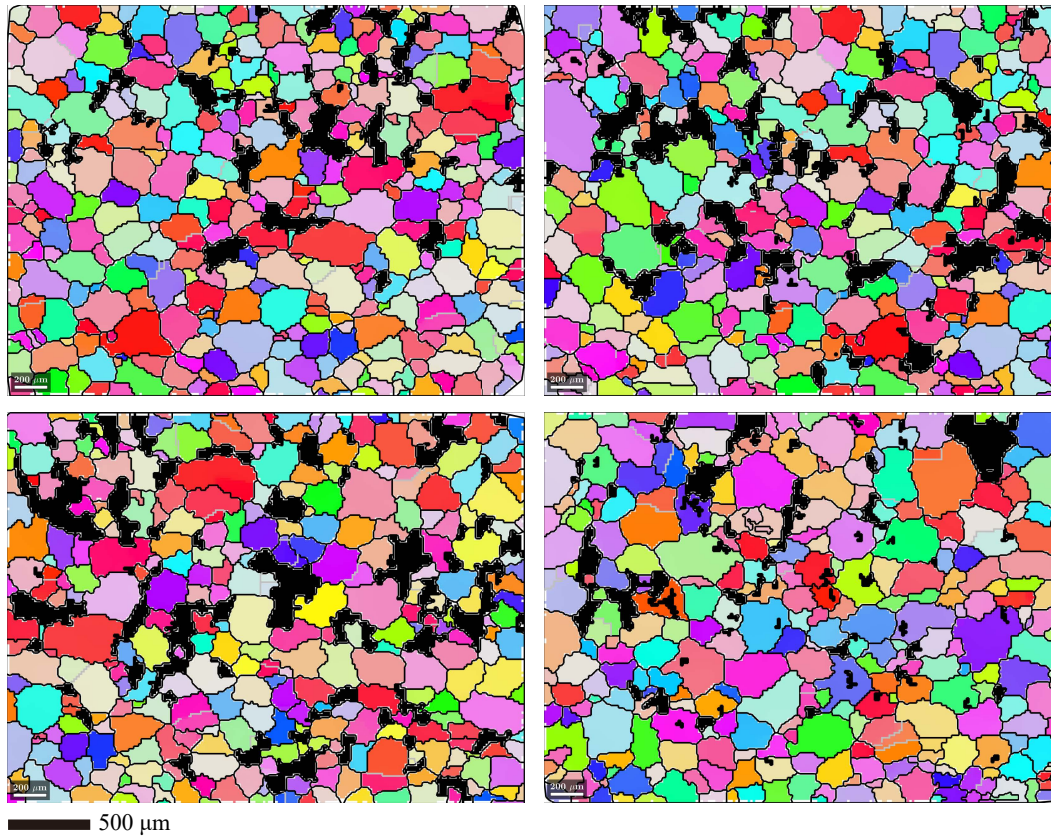


**Figure S3.** Complete microstructure map for the undeformed sample. Orientation maps are colored by the crystallographic orientation normal to the shear plane (IPF-Y, see the color map in Fig. 5 in the main text). Graphite phase detected by EDS is black. Grain boundaries, characterized by a misorientation of  $\geq 10^\circ$ , are black, and subgrain boundaries, characterized by a misorientation of  $< 10^\circ$  and  $\geq 2^\circ$ , are gray.

## ECAP\_33\_1p

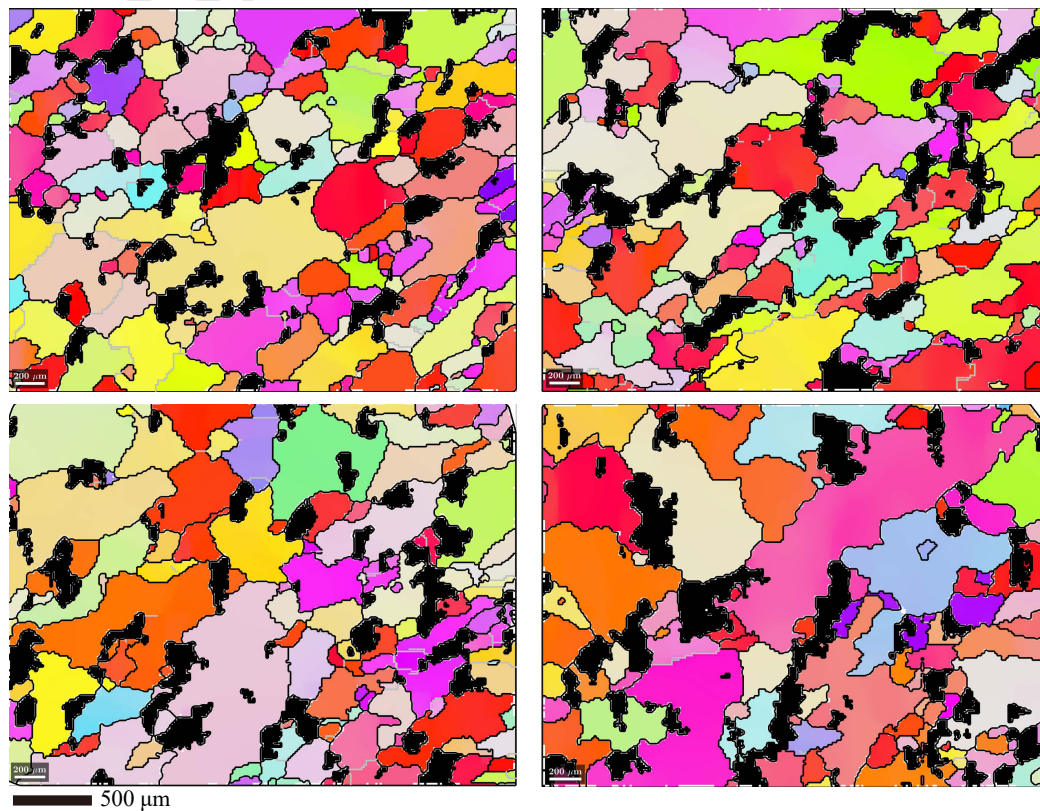


**Figure S4.** Complete set of maps for sample ECAP\_33\_1p. Orientation maps are colored by the crystallographic orientation normal to the shear plane (IPF-Y, see the color map in Fig. 5 in the main text). Graphite phase detected by EDS is black. Grain boundaries, characterized by a misorientation of  $\geq 10^\circ$ , are black, and subgrain boundaries, characterized by a misorientation of  $< 10^\circ$  and  $\geq 2^\circ$ , are gray.

ECAP 19 2p

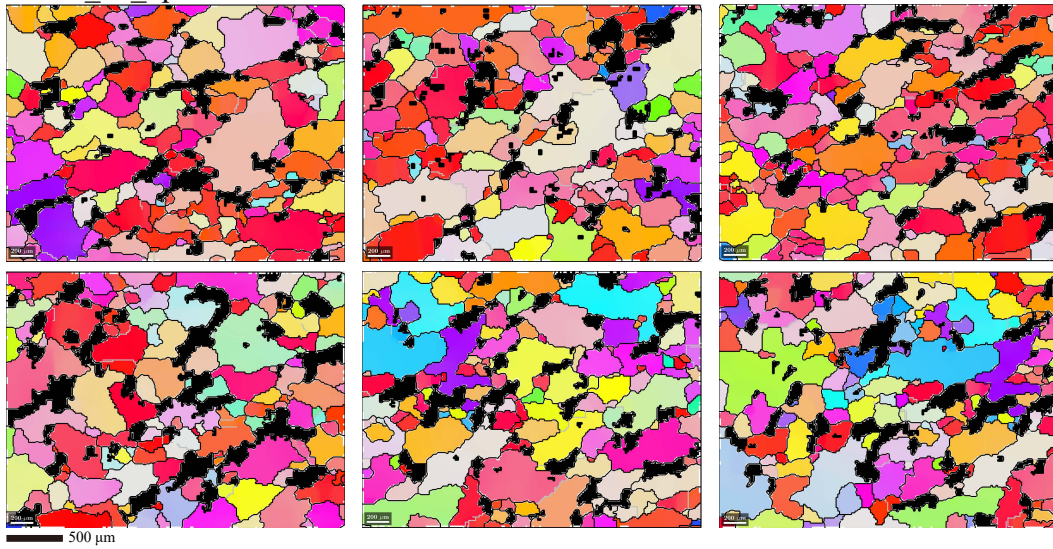


**Figure S5.** Complete microstructure map for sample ECAP\_19\_2p. Orientation maps are colored by the crystallographic orientation normal to the shear plane (IPF-Y, see the color map in Fig. 5 in the main text). Graphite phase detected by EDS is black. Grain boundaries, characterized by a misorientation of  $\geq 10^\circ$ , are black, and subgrain boundaries, characterized by a misorientation of  $< 10^\circ$  and  $\geq 2^\circ$ , are gray.

ECAP\_19\_3p

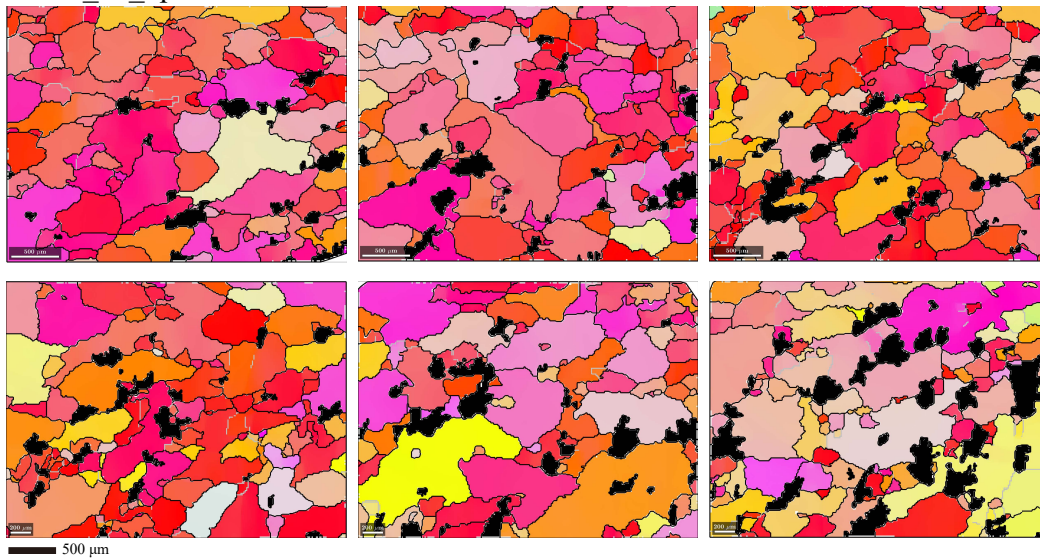


**Figure S6.** Complete microstructure map for sample ECAP\_19\_3p. Orientation maps are colored by the crystallographic orientation normal to the shear plane (IPF-Y, see the color map in Fig. 5 in the main text). Graphite phase detected by EDS is black. Grain boundaries, characterized by a misorientation of  $\geq 10^\circ$ , are black, and subgrain boundaries, characterized by a misorientation of  $< 10^\circ$  and  $\geq 2^\circ$ , are gray.



ECAP 21\_4p

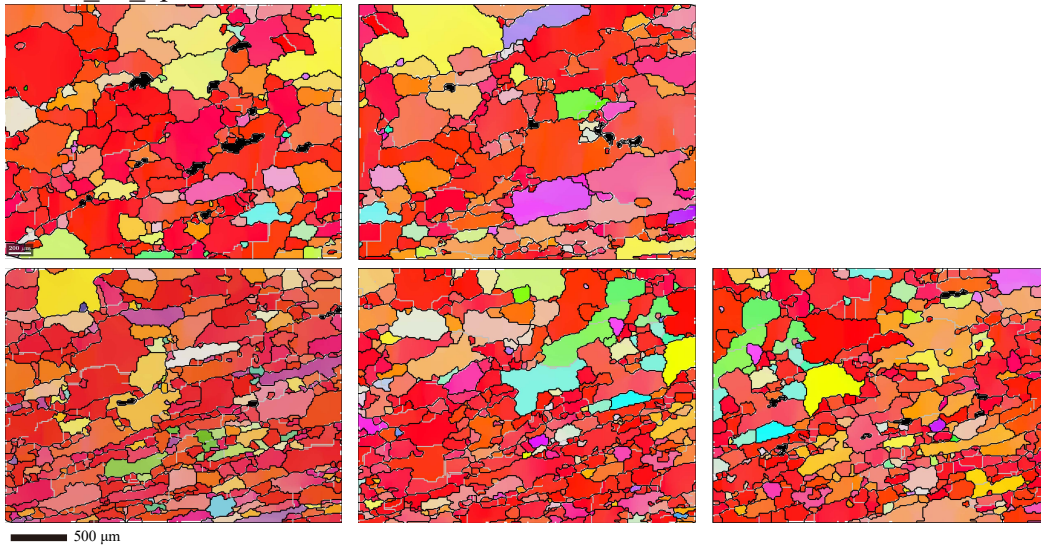


**Figure S7.** Complete microstructure map for sample ECAP\_21\_4p. Orientation maps are colored by the crystallographic orientation normal to the shear plane (IPF-Y, see the color map in Fig. 5 in the main text). Graphite phase detected by EDS is black. Grain boundaries, characterized by a misorientation of  $\geq 10^\circ$ , are black, and subgrain boundaries, characterized by a misorientation of  $< 10^\circ$  and  $\geq 2^\circ$ , are gray.

ECAP\_34\_5p

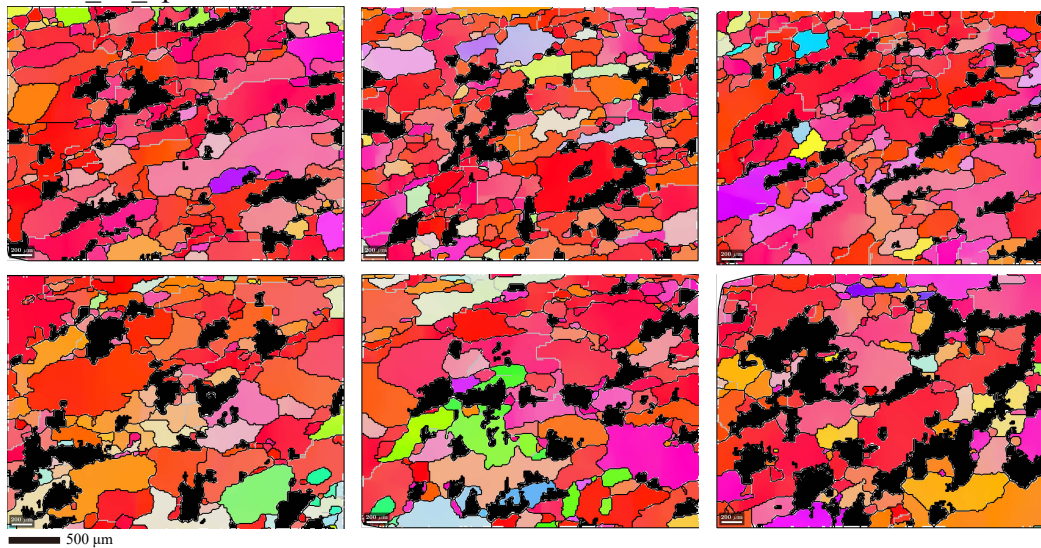


**Figure S8.** Complete microstructure map for sample ECAP\_34\_5p. Orientation maps are colored by the crystallographic orientation normal to the shear plane (IPF-Y, see the color map in Fig. 5 in the main text). Graphite phase detected by EDS is black. Grain boundaries, characterized by a misorientation of  $\geq 10^\circ$ , are black, and subgrain boundaries, characterized by a misorientation of  $< 10^\circ$  and  $\geq 2^\circ$ , are gray.

ECAP\_38\_6p

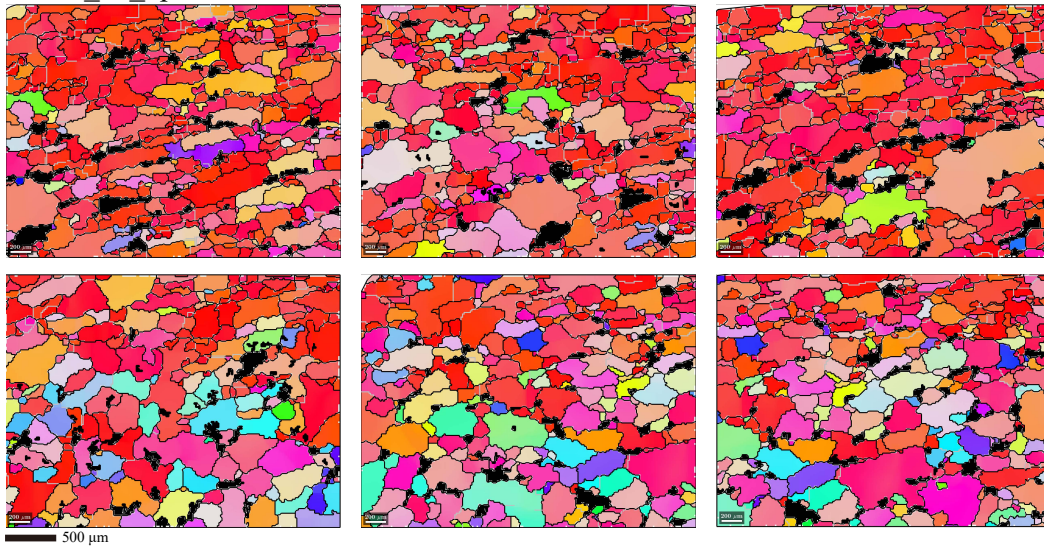


**Figure S9.** Complete microstructure map for sample ECAP\_38\_6p. Orientation maps are colored by the crystallographic orientation normal to the shear plane (IPF-Y, see the color map in Fig. 5 in the main text). Graphite phase detected by EDS is black. Grain boundaries, characterized by a misorientation of  $\geq 10^\circ$ , are black, and subgrain boundaries, characterized by a misorientation of  $< 10^\circ$  and  $\geq 2^\circ$ , are gray.